AIP Advances

Analysis of the optical response of a SARS-CoV-2-directed colorimetric immunosensor

Ⓕ SCI

ⓘD Antonio Minopoli, ⓘD Emanuela Scardapane, ⓘD Adriano Acunzo, ⓘD Raffaele Campanile, ⓘD Bartolomeo Della Ventura, and ⓘD Raffaele Velotta

COLLECTIONS

Ⓕ This paper was selected as Featured

SCI This paper was selected as Scilight
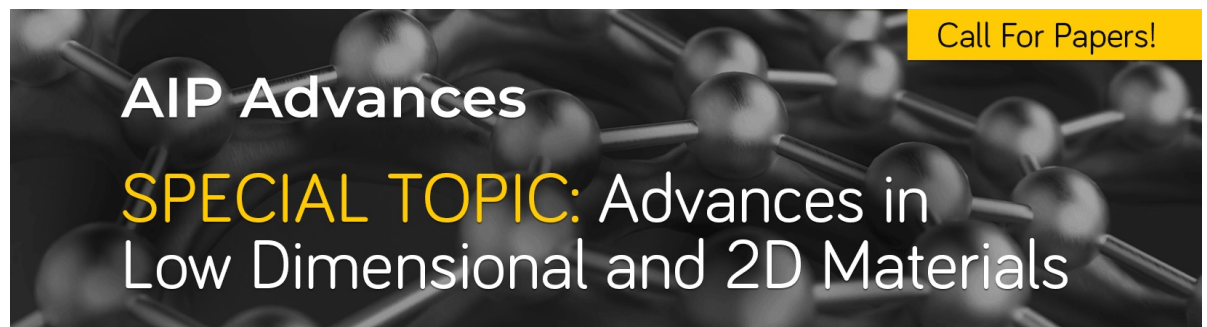
View Online **Export Citation** **CrossMark**

ARTICLES YOU MAY BE INTERESTED IN

Detecting SARS-CoV-2 with a rapid, cost-effective colorimetric biosensor
Scilight **2021**, 251103 (2021); https://doi.org/10.1063/10.0005486

Effect of water models on structure and dynamics of lignin in solution
AIP Advances **11**, 065024 (2021); https://doi.org/10.1063/5.0047974

Integrated nanophotonics for the development of fully functional quantum circuits based on on-demand single-photon emitters
APL Photonics **6**, 010901 (2021); https://doi.org/10.1063/5.0031628

AIP Advances

Call For Papers!

SPECIAL TOPIC: Advances in Low Dimensional and 2D Materials

Analysis of the optical response of a SARS-CoV-2-directed colorimetric immunosensor SCI F

View Online Export Citation CrossMark

Antonio Minopoli, (iD) Emanuela Scardapane, (iD) Adriano Acunzo, (iD)
Raffaele Campanile, (iD) Bartolomeo Della Ventura,[a] (iD) and Raffaele Velotta[a] (iD)

AFFILIATIONS

Department of Physics "E. Pancini," University of Naples Federico II, Via Cintia 26, 80126 Naples, Italy

[a]Authors to whom correspondence should be addressed: bartolomeo.dellaventura@unina.it and rvelotta@unina.it

ABSTRACT

The optical response of different configurations of functionalized gold nanoparticles (f-AuNPs) and SARS-CoV-2 virions is simulated in order to explore the behavior of a colloidal solution containing 10^5–10^{13} virions/ml. The analysis herein reported is carried out for three concentration regimes: (i) low ($\lesssim 10^8$ virions/ml), (ii) intermediate ($\sim 10^9$–10^{10} virions/ml), and (iii) high ($\gtrsim 10^{11}$ virions/ml). Given the high binding effectiveness of f-AuNPs to virions, three different configurations are expected to arise: (i) virions completely surrounded by f-AuNPs, (ii) aggregates (dimers or trimers) of virions linked by f-AuNPs, and (iii) single f-AuNP surrounded by virions. It is demonstrated that 20 nm diameter gold nanoparticles functionalized against all three kinds of SARS-CoV-2 proteins (membrane, envelope, and spike) allow one to reach a limit of detection (LOD) of $\sim 10^6$ virions/ml, whereas the use of only one kind of f-AuNP entails a ten-fold worsening of the LOD. It is also shown that the close proximity (~ 5 nm) of the f-AuNP to the virions assumed throughout this analysis is essential to avoid the hook effect, thereby pointing out the importance of realizing an apt functionalization procedure that keeps thin the dielectric layer (e.g., proteins or aptamers) surrounding the gold nanoparticles.

I. INTRODUCTION

The spread of SARS-CoV-2 all over the world has led the scientific community to put great effort into the quest for alternative strategies that work alongside the real-time reverse transcription polymerase chain reaction (RT-PCR) to detect the virus.[1–4] Although the RT-PCR remains the gold standard to diagnose the presence of the virus, such a technique is laborious and expensive and, hence, not suitable for mass screening. In fact, this molecular assay should be employed only when there is a strong clinical suspicion of infection or in the case of a close contact with a positively confirmed patient.[5] The World Health Organization (WHO) drew up guidelines on the use of antigenic rapid tests, which must have a sensitivity equal to or greater than 80% and a specificity equal to or greater than 97%.[6] A few techniques are available to quickly determine the antigen concentration via both nasopharyngeal secretions[7–10] and saliva,[11,12] providing a quite satisfying overlap with molecular assay results. Most of them rely on the detection of

SARS-CoV-2 proteins or RNA, thereby requiring the virion lysis. Nevertheless, the detection of the lysed proteins or viral RNA, rather than the virion itself, may be detrimental to the correct diagnosis since the capability to selectively distinguish active from inactive viral particles is crucial to assess the actual degree of infectiveness of a specimen.[13]

An alternative to the antigenic tests is the serologic assays based on lateral flow immunochromatographic tests.[14] They are realized to specifically detect antibodies directed to SARS-CoV-2 in patient's blood,[15] but Zhang et al.[16] demonstrated that both immunoglobulins M (IgM) and G (IgG) are detectable only a few days after the contraction of the disease. Therefore, antibody-targeted detection technology is not suitable for screening early infections and it is more useful to monitor the convalescence phase.

Meanwhile, several biosensors have been developed to directly detect the virions, including electrochemical (EC) biosensors,[17] fluorescence-based biosensors,[18] colorimetric biosensors,[7]

surface-enhanced Raman scattering (SERS),[19] and quartz crystal microbalance (QCM).[20] Among them, label-free EC biosensors and SERS are the most popular. These biosensors can be easily miniaturized and mass fabricated; however, they are not for end users since they are expensive and require expert personnel.

Colorimetric biosensors relying upon localized surface plasmon resonance (LSPR) represent a promising strategy to deal with the mass screening challenge since they provide an affordable, reliable, and easy-to-use approach. Although this technology has been widely used to detect different antigens and viruses even before the spread of the current pandemics,[21–23] these biosensors do not usually provide a competitive limit of detection (LOD), and they also run into the hook effect. As shown by Ventura *et al.*,[7] such drawbacks can be addressed by adopting two ingredients: (i) a colloidal solution containing gold nanoparticles functionalized (f-AuNPs) against all three kinds of SARS-CoV-2 proteins (membrane, envelope, and spike) and (ii) the photochemical immobilization technique (PIT) able to covalently tether antibodies onto gold surfaces in a well-oriented way.[24]

In this work, we describe the optical response of a colorimetric immunosensor based on the specific aggregation of 20 nm diameter gold nanoparticles in a colloidal solution containing 3×10^{11} f-AuNPs (anti-membrane, anti-envelope, and anti-spike f-AuNPs in the ratio 1:1:1) and 10^5–10^{13} virions/ml.[7] To this aim, we use the finite-difference time-domain (FDTD) method to simulate the optical response of different configurations of f-AuNPs and SARS-CoV-2 virions inferring the interaction mechanisms at the nanoscale in various concentration regimes. We demonstrated that the adoption of the aforementioned mix of photochemically f-AuNPs allowed us not only to reach a remarkable LOD of 10^6 virions/ml but also to prevent the hook effect.

II. FDTD NUMERICAL SIMULATION

A. Method

The optical response of different complexes of SARS-CoV-2 virions and f-AuNPs was simulated by the "FDTD solutions" tool implemented in Lumerical software. The tool relies on the FDTD method to solve Maxwell's equations inside the unit volumes a simulation workspace is discretized into. Figure 1 shows the scheme of the workspace we employed for all the simulations. Each complex was placed in a total-field scattered-field (TFSF) volume that allows us to discriminate the transmitted light from the scattering contribution.

First, a source of *x*-polarized electromagnetic waves traveling along the *z* direction and whose wavelengths lied in the range of 400–800 nm invested the target of interest. Then, the transmitted and forward-scattered light were both collected by a total field photodetector (spectral resolution: 1 nm) placed on the TFSF facet opposite to that hosting the source, whereas the whole scattered light *S* was recorded by a scattered field photodetector box placed all around the TFSF region (spectral resolution: 1 nm). Thus, we could retrieve the transmittance by subtracting the forward-scattering contribution S_f measured on the forward facet of the photodetector box from the total signal recorded by the photodetector placed inside the TFSF volume. Therefore, the extinction *E* is calculated as
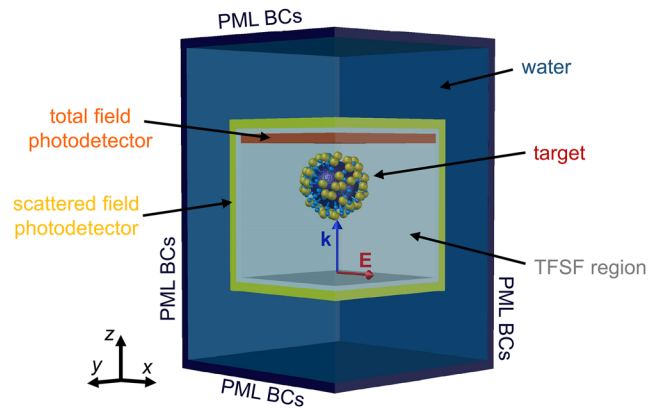

FIG. 1. Sketch of the simulation workspace consisting of the *x*-polarized plane wave source, target, embedding medium (water), total field photodetector (orange panel), TFSF region (white box), scattered field photodetector (yellow box), and PML BCs (blue box).

$$E = -\log\left(\frac{I}{I_0}\right) + S_f, \qquad (1)$$

where I_0 is the source intensity and I is the light intensity measured on the total field photodetector. The absorbance is defined as $A = E - S$. The corresponding cross sections σ are defined as

$$\sigma_{ext} = \frac{E}{n l_t}, \qquad (2)$$

$$\sigma_{sca} = \frac{S}{n l_s}, \qquad (3)$$

$$\sigma_{abs} = \sigma_{ext} - \sigma_{sca}, \qquad (4)$$

where n is the number density of the targets, l_t is the distance between the source and total field photodetector, and l_s is the penetration depth from the source to the scattered field photodetector.

The TFSF region was embedded into a FDTD simulation volume filled by water with a refractive index of 1.33. Perfect matched layer (PML) boundary conditions (BCs) were set along all directions to ensure the perfect absorption of the electromagnetic radiation propagating in the far field without creating any back reflections.[25] Since the PML BCs require that the distance between TFSF and FDTD boundaries is at least $\lambda_{max}/2$, where λ_{max} is the maximum value of the source wavelength, we set the simulation volume 500 nm larger (in all directions) than the TFSF size. Finally, the workspace was discretized over a spatial mesh (1 nm) dense enough to warrant high accuracy of the results while keeping reasonable the simulation time.

The virion was modeled as a homogeneous sphere of 100 nm diameter and refractive index 1.75[26] surrounded by 2000 dots of refractive index 1.45 to simulate the membrane proteins,[27] 20 dots for the envelope proteins,[27] and 100 cylinders 10 nm high with a refractive index of 1.45 to mimic the spike proteins.[27] Gold nanoparticles were modeled as a homogeneous gold sphere of 20 nm diameter whose optical properties were taken by CRC Handbook of Chemistry and Physics,[28] whereas the antibodies anchored to the gold

surface were modeled as a dielectric shell with a refraction index of 1.42[29] and a thickness of 5 nm,[23] the latter arising in case a functionalization procedure such as PIT is adopted.[24] Functionalized AuNPs were randomly arranged onto both the virion envelope and spike proteins, thereby giving rise to double layers of nanoparticles.

B. Extinction of SARS-CoV-2 and f-AuNPs complexes

We intended to investigate the optical behavior of a 1 ml colloidal solution containing $N = 3 \times 10^{11}$ gold nanoparticles of 20 nm

diameter functionalized to obtain three kinds of f-AuNPs (anti-membrane, anti-envelope, and anti-spike in the ratio 1:1:1) and 10^5–10^{13} virions/ml. To this aim, we simulated the optical response of four configurations of f-AuNPs and virions that could occur in the colloidal solution according to the virion concentration (Fig. 2): (i) virion completely surrounded by f-AuNPs, (ii) virion dimer partially covered by f-AuNPs, (iii) virion trimer covered by a much fewer number of f-AuNPs, and (iv) single f-AuNP surrounded by virions.

Figure 2(a) shows the maximally packed configuration of f-AuNPs around the single virion reasonably emerging when the

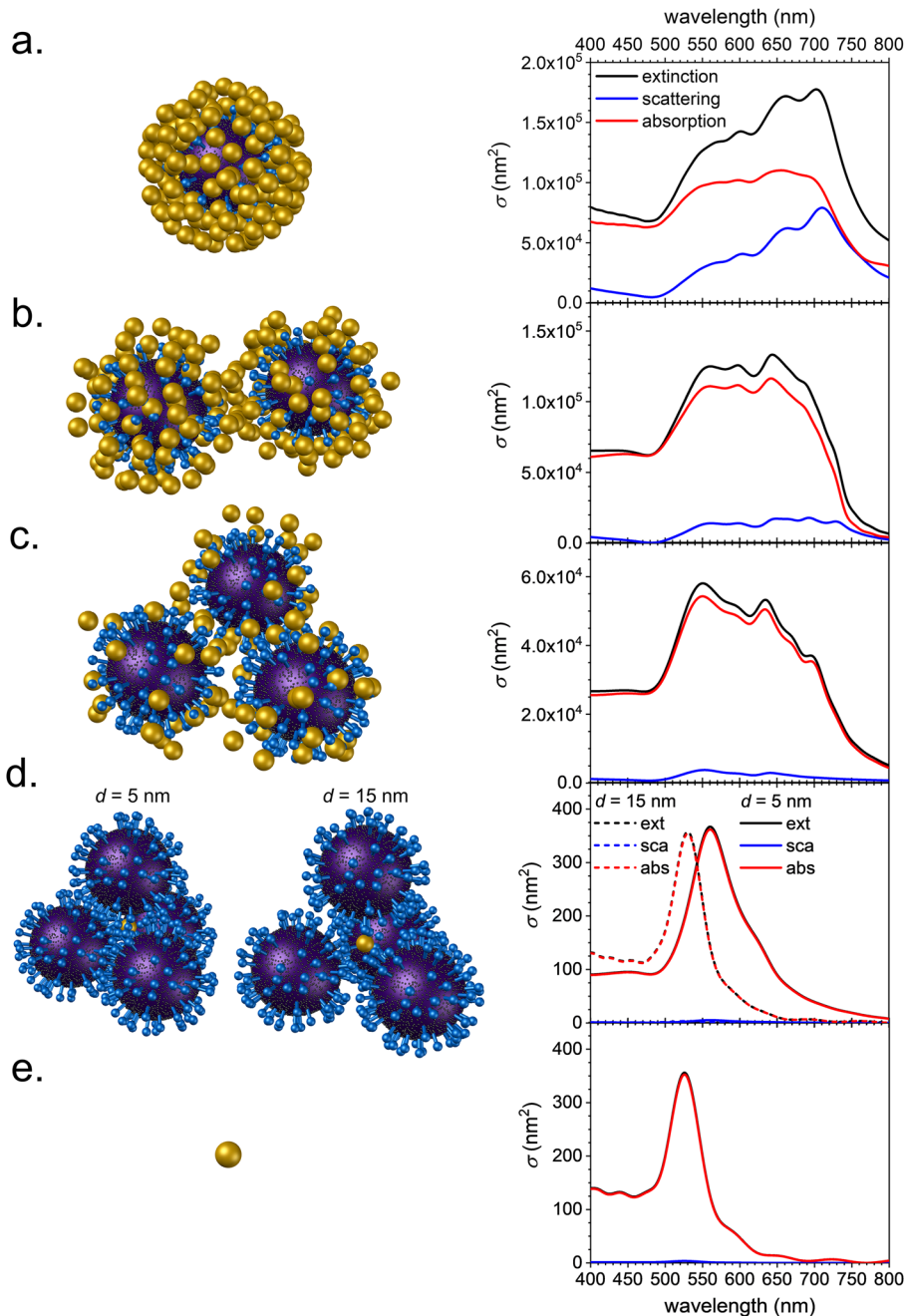FIG. 2. Sketch of the complex (left panel) and corresponding extinction (black solid line), scattering (blue solid line), and absorption (red solid line) cross sections (right panel) for different complex configurations: (a) virion completely surrounded by f-AuNPs, (b) virion dimer partially covered by f-AuNPs, (c) virion trimer covered by a much fewer number of f-AuNPs, (d) single f-AuNP surrounded by virions, and (e) single f-AuNP.

ratio between the number of f-AuNPs and that of virions in the solution is at least 10^3. Here, a number of 80 f-AuNPs were arranged around the virion to completely cover the spherical surface (binding to the membrane and envelope proteins) and 100 f-AuNPs were positioned on the top of the spike proteins. The extinction cross section (black solid line) exhibits a broad LSPR lying in the range of 650–700 nm of ~1.8×10^5 nm^2 at a 700 nm wavelength. Such a value is suitable to produce a detectable signal of 0.002 optical density (OD) if the transmittance of a standard 10 mm cuvette containing 10^6 complexes in 1 ml of aqueous solution is measured. Given the close-packed configuration of the f-AuNPs around the virion, the average interparticle distance turned out to be 8 nm, which is small enough to promote the optical coupling among the nearest neighbors. This led to a large red-shift of the LSPR peak as compared to that of the single f-AuNP at 525 nm [Fig. 2(e)]. Moreover, such a configuration yields a Mie efficiency η of 3.14, where η is defined as

$$\eta = \frac{\sigma_{ext}}{N_b \pi r^2}, \qquad (5)$$

where N_b is the number of f-AuNPs bound to the virion and r is the nanoparticle radius. It is worth noticing that although the scattering cross section of a single f-AuNP of 20 nm diameter is vanishingly small at the LSPR peak (~5 nm^2) (blue solid line in Figs. 2(e),[30] the formation of optical dimers or longer nanoparticle chains entailed an enhancement of σ_{sca} of ~90-fold.[31]

Figure 2(b) shows an intermediate scenario in which the number of f-AuNPs is 10^2–10^3 times the number of virions in the colloidal solution. In this case, each virion can be partially covered by f-AuNPs, and hence, it is reasonable that the formation of dimers of virions held together by shared f-AuNPs be a favorite process. The optical response of the system was worked out by considering 40 f-AuNPs tethered onto the spherical surface and 50 f-AuNPs bound to the spike proteins for each virion. While the absorbance cross section (red solid line) is roughly constant as compared to the close-packed configuration [red solid line in Fig. 2(a)], the scattering cross section (blue solid line) results to be lower (20 times higher than the σ_{sca} of a single 20 nm size f-AuNP) due to the increase in the average interparticle distance (18 ± 12 nm), thereby yielding a Mie efficiency of η = 2.36. The extinction cross section (black solid line) approaches a value of 1.3×10^5 nm^2, which results to be roughly constant in the range of 550–670 nm.

Figure 2(c) shows a possible transient configuration arising whenever 10^{10} virions/ml are in the colloidal solution. In this regime, only a few tens of f-AuNPs are available to bind to each virion on average, thereby promoting larger complexes in which f-AuNPs act as multiple anchoring sites. We simulated a trimer of virions hosting 30 f-AuNPs each (20 f-AuNPs tethered to membrane and envelope proteins and 10 to the spikes). As expected, since the optical coupling among f-AuNPs is weakened by the larger interparticle distance (40 ± 30 nm), the LSPR wavelength (λ_{LSPR}) blue-shifted with respect to the previous (more packed) configurations, while the σ_{sca} became vanishingly small. Thus, the σ_{ext} at λ_{LSPR} is only slightly higher (η = 1.92) than the σ_{abs} resulting from a system of 90 optically decoupled f-AuNPs.

When the number of virions is comparable to or higher than that of nanoparticles, it is reasonable that each f-AuNP can bind to several virions simultaneously. Thus, we explored the optical response in this regime by simulating f-AuNPs enclosed into a tetrahedron of virions. Considering that the colloidal solution contained f-AuNPs directed against all three kinds of SARS-CoV-2 proteins, two possible configurations can arise [Fig. 2(d)]: (i) anti-envelope/anti-membrane f-AuNP enclosed into the tetrahedron in such a way that the separation distance between the nanoparticle and the virion surface is 5 nm and (ii) anti-spike f-AuNP bound to the spike proteins with a separation distance of 15 nm from the virion surface.

In case (i), since the nanoparticle is in close proximity to a relatively high refractive index, the simulated extinction spectrum exhibits a narrow LSPR peak at a 560 nm wavelength being red-shifted as compared to that worked out for the single f-AuNP (525 nm) [Fig. 2(e)]. Here, σ_{ext} reaches 367 nm^2 at 560 nm, leading to η = 1.17. In case (ii), the nanoparticle is too far from the virion surface to be affected by its relatively high refractive index. Thus, the optical response of this complex provides a λ_{LSPR} of 530 nm being quite similar to that exhibited by a single f-AuNP embedded in water [Fig. 2(e)].

C. Calibration curve

Starting from the aforementioned results referring to individual complexes, the optical response of a 1 ml colloidal solution containing a much higher number of complexes and free f-AuNPs was deduced. Figure 3(a) shows the extinction spectra of the colloidal solution obtained by summing the extinction of N_c complexes to the extinction of N_f f-AuNPs, where N_c is the number of complexes in the solution and N_f is the number of free nanoparticles calculated as $N_f = N - N_c N_b$. The optical behavior of the single f-AuNP dominates over the extinction arising from N_c complexes [shown in Fig. 2(a)] as long as the ratio $N_f/N_c \gtrsim 10^3$. In this regime, the right tale of the spectrum raises while the complex concentration increases without significantly red-shifting the LSPR peak at 525 nm (from the violet to cyan solid line in Fig. 3(a).

When the colloidal solution is depleted of free f-AuNPs due to the relatively high virion concentration (10^9–10^{10} virions/ml), the contribution of N_c complexes [shown in Figs. 2(b) and 2(c)] to the extinction emerges, giving rise to a broader and red-shifted spectrum [green and yellow solid lines in Fig. 3(a)].

Finally, at virion concentrations larger than 10^{11} per ml, no free f-AuNPs are in the solution anymore. Thus, the response is ascribable to the complexes shown in Fig. 2(d), thereby exhibiting a narrowing and a blue-shift of the spectrum [from orange to dark red solid lines in Fig. 3(a)] as compared to the intermediate configurations (green and yellow lines). Since the colloidal solution contained the three kinds of f-AuNPs in the ratio 1:1:1, these spectra were retrieved by considering a weighted average of the extinction spectra reported in Fig. 2(d), using a weight of 2/3 for configuration (i) while a weight of 1/3 for configuration (ii).

Figure 3(b) shows the optical density at four specific wavelengths as a function of the virion concentration. The readings at 520 nm (dashed green line), 600 nm (dashed-dotted red line), and 650 nm (dotted dark red line) exhibit a hook effect due to the trend reversal of the λ_{LSPR} shift as soon as the virion concentration becomes comparable to or higher than that of the f-AuNPs ($\gtrsim 10^{11}$ virions/ml). On the contrary, the reading at 560 nm (orange solid
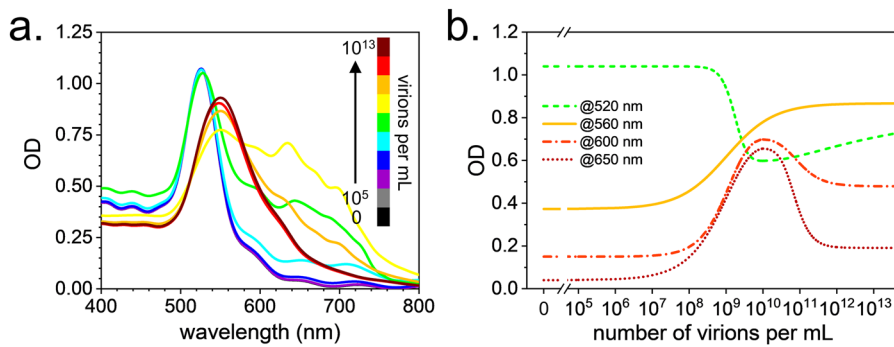
FIG. 3. (a) Extinction spectra of the colloidal solution containing a virion concentration (number of virions/ml) of 0 (black solid line, not visible), 10^5 (gray solid line, not visible), 10^6 (violet solid line), 10^7 (blue solid line), 10^8 (cyan solid line), 10^9 (green solid line), 10^{10} (yellow solid line), 10^{11} (orange solid line), 10^{12} (red solid line), and 10^{13} (dark red solid line). (b) OD readings at 520 nm (green dashed line), 560 nm (orange solid line), 600 nm (dashed-dotted red line), and 650 nm (dotted dark red solid line).

line) is a monotonic function of the virion concentration, and hence, no hook effect takes place.

D. Alternative configurations

Some critical features were explored to corroborate previous assumptions. First, we loosened the constraint of using all three kinds of f-AuNPs (against envelope, membrane, and spike proteins) by considering only one kind at a time. Figure 4(a) represents the virion surrounded by 80 anti-membrane f-AuNPs. The extinction cross section exhibits a peak of 7×10^4 nm^2 at 646 nm, which is blue-shifted with respect to that obtained by adopting all kinds of f-AuNPs. Although the scattering cross section is 55 times larger than that of the single f-AuNP (20 nm diameter) [blue solid line in Fig. 2(e)] and the Mie efficiency is relatively high ($\eta = 2.79$), the optical density at λ_{LSPR} becomes detectable

(OD > 0.001) only when $N_c \geq 10^7$ complexes per ml. Therefore, the adoption of a colloidal solution containing only anti-membrane f-AuNPs entails a worsening of the LOD of one order of magnitude.

Similarly, the extinction resulting from the virion surrounded by 100 anti-spike f-AuNPs (6.9×10^4 nm^2 at 552 nm) [Fig. 4(b)] is not sufficient to produce a detectable signal with 10^6 virions/ml and a ten-fold worsening of the LOD occurs. Note that the configuration arising from the virion surrounded by 20 anti-envelope f-AuNPs was not investigated since its extinction would be further damped as compared to the case of only anti-membrane f-AuNPs due to both the lower number of nanoparticles and the larger interparticle distance.

Thus, aiming at achieving such a remarkable LOD of 10^6 virions/ml, it was necessary to maximize the covering of the virions by employing f-AuNPs functionalized against all the SARS-CoV-2
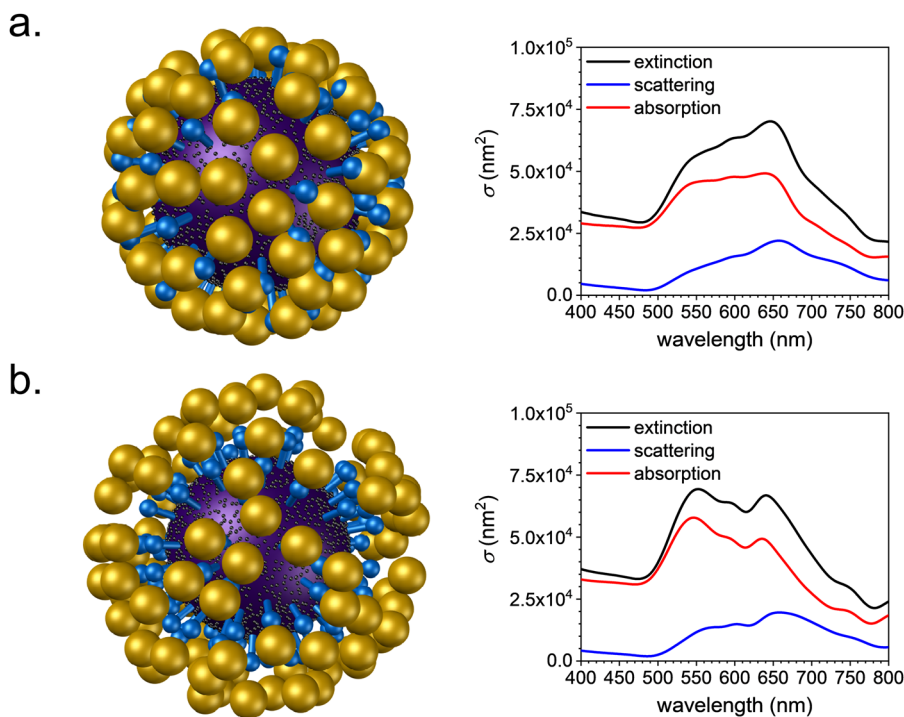

FIG. 4. Sketch of the complex (left panel) and corresponding extinction (black solid line), scattering (blue solid line), and absorption (red solid line) cross sections (right panel) for the (a) virion surrounded by anti-membrane f-AuNPs and (b) virion surrounded by anti-spike f-AuNPs.
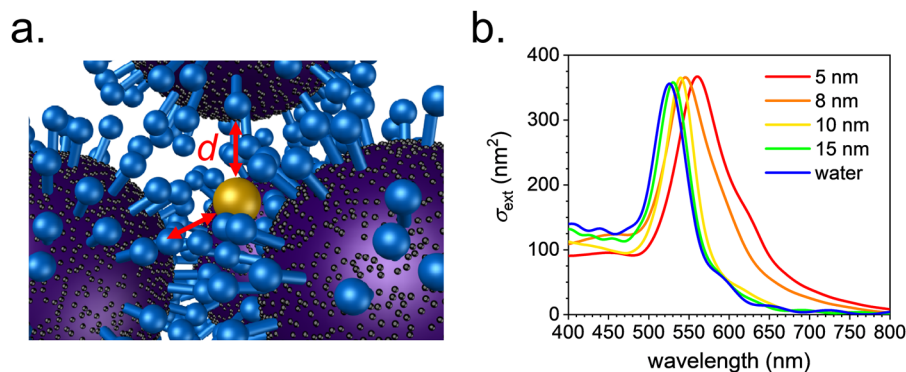
FIG. 5. (a) Magnification of the tetrahedron complex with nanoparticle–virion separation distances highlighted by red double arrows. (b) Extinction cross section worked out for 5 nm (red solid line), 8 nm (orange solid line), 10 nm (yellow solid line), and 15 nm (green solid line) separation distances between the f-AuNPs and the embedding virions.

proteins so as to increase as much as possible the extinction of the complexes.

Second, we simulated the optical response of the complexes at a high virion concentration ($\gtrsim 10^{11}$ virions/ml) by varying the separation distance between the f-AuNP and virion surface in order to investigate the role played by the separation distance. For instance, we took into account some possible configurations with a larger separation distance that would emerge from other antibody functionalization techniques (e.g., self-assembled monolayer as mediators to create thiol–gold link for protein A/G as antibody anchors). Figure 5(a) shows a magnification of the tetrahedron complex highlighting the separation distance between the f-AuNP and virion surface, whereas the extinction spectra obtained by considering some separation distances from 5 to 15 nm are reported in Fig. 5(b). Since the plasmonic properties of metal nanostructures strongly depend on the refractive index of the surrounding medium,[32] λ_{LSPR} blue-shifts as the nanoparticle–virion distance increases, approaching the extinction spectrum of the single f-AuNP (20 nm diameter) embedded in water. The behavior of the LSPR shift λ_{LSPR} as a function of the separation distance is described by the exponential curve,[33]

$$\lambda_{LSPR} = k e^{-\frac{x}{l}}, \tag{6}$$

where $k = 90 \pm 3$ nm, while $l = 5.3 \pm 0.2$ is the decay length of the localized surface plasmon. Therefore, if the functionalization technique entails a separation distance larger than ~15 nm, a hook effect takes place at very high virion concentrations even when the OD reading is taken at 560 nm.

III. CONCLUSIONS

Herein, it is demonstrated that the adoption of a colloidal solution containing a mix of f-AuNPs against SARS-CoV-2 envelope, membrane, and spike proteins warrants a detectable signal down to ~10^6 virions/ml.[7] Such a remarkable LOD turns out to be at least one order of magnitude lower as compared to a similar colorimetric approach relying on aptamer-functionalized gold nanoparticles for detecting Zika virus.[34]

Although there is a lack of the plasmon coupling among f-AuNPs at high virion concentrations, no hook effect occurs when the separation distance between the f-AuNP and the virion is kept small ($\lesssim 5$ nm). Such a feature can be realized by appropriate functionalization procedures such as PIT.[24] Indeed, such a technique guarantees the minimal separation distance between the f-AuNP and

virion surface and, hence, the trend reversal of the λ_{LSPR} shift at high virion concentrations (hook effect) does not take place since the f-AuNPs are affected by the relatively high refractive index of the virions. This feature is of fundamental importance in the current pandemics since rapid antigenic tests are mainly meant to seek for people with very high viral loads (so-called superspreaders), which would fall in the false negatives in the case of the occurrence of the hook effect.

DATA AVAILABILITY

The data that support the findings of this study are available from the corresponding authors upon reasonable request.

REFERENCES

[1] R. Lassaunière, A. Frische, Z. B. Harboe, A. C. Nielsen, A. Fomsgaard, K. A. Krogfelt, and C. S. Jørgensen, Medrxiv:20056325 (2020).

[2] Ö. Appak, M. Duman, N. Belet, and A. A. Sayiner, J. Med. Virol. **91**, 731 (2019).

[3] P. D. Skottrup, M. Nicolaisen, and A. F. Justesen, Biosens. Bioelectron. **24**, 339 (2008).

[4] J. Xia, J. Tong, M. Liu, Y. Shen, and D. Guo, J. Med. Virol. **92**, 589 (2020).

[5] U.S. Centers for Disease Control and Prevention, "CDC 2019-Novel Coronavirus(2019-nCoV) real-time RT-PCR diagnostic panel for emergency use only," https://www.fda.gov/media/134922/download, 1 December 2020.

[6] World Health Organization, "WHO Interim Guidance 11 September 2020. Antigen-detection in the diagnosis of SARS-CoV-2 infection using rapid immunoassays," WHO/2019-nCoV/Antigen_Detection/2020.1, https://apps.who.int/iris/bitstream/handle/10665/334253/WHO-2019-nCoV-Antigen_Detection-2020.1-eng.pdf?sequence=1&isAllowed=y (2020).

[7] B. Della Ventura, M. Cennamo, A. Minopoli, R. Campanile, S. Bolletti Censi, D. Terracciano, G. Portella, and R. Velotta, ACS Sens. **5**, 3043 (2020).

[8] J. Alcoba-Florez, R. González-Montelongo, A. Íñigo-Campos, D. G.-M. de Artola, H. Gil-Campesino, L. Ciuffreda, A. Valenzuela-Fernández, C. Flores, and Microbiology Technical Support Team, Int. J. Infect. Dis. **97**, 66 (2020).

[9] L. Yu, S. Wu, X. Hao, X. Li, X. Liu, S. Ye, H. Han, X. Dong, X. Li, J. Li, N. Liu, J. Liu, W. Zhang, V. Pelechano, W. H. Chen, and X. Yin, Medrxiv: https://doi.org/10.1101/2020.02.20.20025874 (2020).

[10] E. Adams, M. Ainsworth, R. Anand, M. I. Andersson, K. Auckland, J. K. Baillie, E. Barnes, S. Beer, J. I. Bell, T. Berry, S. Bibi, M. Carroll, S. K. Chinnakannan, E. Clutterbuck, R. J. Cornall, D. W. Crook, T. de Silva, W. Dejnirattisai, K. E. Dingle, C. Dold, A. Espinosa, D. W. Eyre, H. Farmer, M. F. Mendoza, D. Georgiou, S. J. Hoosdally, A. Hunter, K. Jeffery, D. Kelly, P. Klenerman, J. Knight, C. Knowles, A. J. Kwok, U. Leuschner, R. Levin, C. Liu, C. López-Camacho, J. Martinez, P. C. Matthews, H. McGivern, A. J. Mentzer, J. Milton, J. Mongkolsapaya, S. C. Moore, M. S. Oliveira, F. Pereira, E. Perez, T. Peto, R. J. Ploeg, A. Pollard, T. Prince, D. J. Roberts, J. K. Rudkin, V. Sanchez,

G. R. Screaton, M. G. Semple, J. Slon-Campos, D. T. Skelly, E. N. Smith, A. Sobrinodiaz, J. Staves, D. I. Stuart, P. Supasa, T. Surik, H. Thraves, P. Tsang, L. Turtle, A. S. Walker, B. Wang, C. Washington, N. Watkins, and J. Whitehouse, Medrxiv: https://doi.org/10.1101/2020.04.15.20066407 (2020).

[11] A. L. Wyllie, J. Fournier, A. Casanovas-Massana, M. Campbell, M. Tokuyama, P. Vijayakumar, B. Geng, M. C. Muenker, A. J. Moore, C. B. F. Vogels, M. E. Petrone, I. M. Ott, P. Lu, A. Venkataraman, A. Lu-Culligan, J. Klein, R. Earnest, M. Simonov, R. Datta, R. Handoko, N. Naushad, L. R. Sewanan, J. Valdez, E. B. White, S. Lapidus, C. C. Kalinich, X. Jiang, D. J. Kim, E. Kudo, M. Linehan, T. Mao, M. Moriyama, J. E. Oh, A. Park, J. Silva, E. Song, T. Takahashi, M. Taura, O. El Weizman, P. Wong, Y. Yang, S. Bermejo, C. Odio, S. B. Omer, C. S. Dela Cruz, S. Farhadian, R. A. Martinello, A. Iwasaki, N. D. Grubaugh, and A. I. Ko, Medrxiv: https://doi.org/10.1101/2020.04.16.20067835 (2020).

[12] L. Azzi, G. Carcano, F. Gianfagna, P. Grossi, D. D. Gasperina, A. Genoni, M. Fasano, F. Sessa, L. Tettamanti, F. Carinci, V. Maurino, A. Rossi, A. Tagliabue, and A. Baj, J. Infect. **81**, e45 (2020).

[13] P. Moitra, M. Alafeef, K. Dighe, M. B. Frieman, and D. Pan, ACS Nano **14**, 7617 (2020).

[14] Z. Li, Y. Yi, X. Luo, N. Xiong, Y. Liu, S. Li, R. Sun, Y. Wang, B. Hu, W. Chen, Y. Zhang, J. Wang, B. Huang, Y. Lin, J. Yang, W. Cai, X. Wang, J. Cheng, Z. Chen, K. Sun, W. Pan, Z. Zhan, L. Chen, and F. Ye, J. Med. Virol. **92**, 1518 (2020).

[15] K. K.-W. To, O. T.-Y. Tsang, W.-S. Leung, A. R. Tam, T.-C. Wu, D. C. Lung, C. C.-Y. Yip, J.-P. Cai, J. M.-C. Chan, T. S.-H. Chik, D. P.-L. Lau, C. Y.-C. Choi, L.-L. Chen, W.-M. Chan, K.-H. Chan, J. D. Ip, A. C.-K. Ng, R. W.-S. Poon, C.-T. Luo, V. C.-C. Cheng, J. F.-W. Chan, I. F.-N. Hung, Z. Chen, H. Chen, and K.-Y. Yuen, Lancet Infect. Dis. **20**, 565 (2020).

[16] W. Zhang, R.-H. Du, B. Li, X.-S. Zheng, X.-L. Yang, B. Hu, Y.-Y. Wang, G.-F. Xiao, B. Yan, Z.-L. Shi, and P. Zhou, Emerging Microbes Infect. **9**, 386 (2020).

[17] L. A. Layqah and S. Eissa, Microchim. Acta **186**, 224 (2019).

[18] H. M. Froggatt, B. E. Heaton, and N. S. Heaton, J. Virol. **94**, e01265–20 (2020).

[19] S. A. Jadhav, P. Biji, M. K. Panthalingal, C. Murali Krishna, S. Rajkumar, D. S. Joshi, and N. Sundaram, Med. Hypotheses **146**, 110356 (2021).

[20] L. M. Pandey, Expert Rev. Proteomics **17**, 425 (2020).

[21] M. Iarossi, C. Schiattarella, I. Rea, L. De Stefano, R. Fittipaldi, A. Vecchione, R. Velotta, and B. Della Ventura, ACS Omega **3**, 3805 (2018).

[22] Y. Liu, L. Zhang, W. Wei, H. Zhao, Z. Zhou, Y. Zhang, and S. Liu, Analyst **140**, 3989 (2015).

[23] A. Minopoli, N. Sakač, B. Lenyk, R. Campanile, D. Mayer, A. Offenhäusser, R. Velotta, and B. Della Ventura, Sens. Actuators, B **308**, 127699 (2020).

[24] B. Della Ventura, M. Banchelli, R. Funari, A. Illiano, M. De Angelis, P. Taroni, A. Amoresano, P. Matteini, and R. Velotta, Analyst **144**, 6871 (2019).

[25] J.-P. Bérenger, Synth. Lect. Comput. Electromagn. **2**, 1 (2007).

[26] I. Makra, P. Terejánszky, and R. E. Gyurcsányi, MethodsX **2**, 91 (2015).

[27] Y. M. Bar-On, A. Flamholz, R. Phillips, and R. Milo, eLife **9**, e57309 (2020).

[28] W. M. Haynes, *CRC Handbook of Chemistry and Physics* (CRC Press, 2016).

[29] N. C. Bell, C. Minelli, and A. G. Shard, Anal. Methods **5**, 4591 (2013).

[30] P. K. Jain, K. S. Lee, I. H. El-Sayed, and M. A. El-Sayed, J. Phys. Chem. B **110**, 7238 (2006).

[31] M. Loumaigne, C. Midelet, T. Doussineau, P. Dugourd, R. Antoine, M. Stamboul, A. Débarre, and M. H. V. Werts, Nanoscale **8**, 6555 (2016).

[32] K. M. Mayer, J. H. Hafner, and A. À. Antigen, Chem. Rev. **111**, 3828 (2011).

[33] P. K. Jain, W. Huang, and M. A. El-Sayed, Nano Lett. **7**, 2080 (2007).

[34] A. Bosak, N. Saraf, A. Willenberg, M. W. C. Kwan, B. W. Alto, G. W. Jackson, R. H. Batchelor, T. D. Nguyen-Huu, V. Sankarapani, G. D. Parks, S. Seal, and B. J. Willenberg, RSC Adv. **9**, 23752 (2019).